

Chapter 18. Processes at the Ice Edge – The Arctic

Robert A. Shuchman

Altarum (formerly ERIM), Ann Arbor, Michigan, USA

Robert G. Onstott

General Dynamics - Advanced Information Systems, Ann Arbor, Michigan, USA

Ola M. Johannessen

Nansen Environmental and Remote Sensing Center (NERSC), Bergen, Norway

Stein Sandven

Nansen Environmental and Remote Sensing Center (NERSC), Bergen, Norway

Johnny A. Johannessen

Nansen Environmental and Remote Sensing Center (NERSC), Bergen, Norway

18.1 Introduction

At the margin of the sea ice cover (the edge), the abrupt transition to open water gives rise to unique processes including water mass formation, oceanic upwelling, wave propagation into the ice, eddy formation and atmospheric boundary layer processes [e.g., *Muench, et al.*, 1987]. The ice extent, the latitude of the ice edge as a function of longitude, is both of climatological and practical importance. Annual variation of sea ice extent is carefully observed as an early indication of greenhouse-induced climate change [*Stouffer, et al.*, 1989]. Monitoring the ice extent and variability of the ice edge is important for practical reasons such as sea traffic, fisheries, offshore operations and other military marine activities in ice edge regions.

This chapter discusses specific Marginal Ice Zone (MIZ) characteristics observable from synthetic aperture radar (SAR). First, the determination of the ice open water boundary will be discussed. An overview of SAR observations of eddies and of new ice formation at the ice edge, such as the Odden event in the Greenland/Iceland/Norwegian Sea, follows. Examples of gravity wave propagation into the ice are presented and some characteristic ice processes in the Kara Sea region are described at the end of the chapter. Discussion of the Northern Sea Route in the Kara Sea area further illustrates ice edge processes and conditions as they affect shipping, and shows how a range of ice conditions are represented in SAR imagery. In this case, the ice edge is defined by polynyas or leads (open water) in the ice.

18.2 Ice Edge Characteristics

The ice edge is the demarcation at any given time between the open water and sea ice of any kind. It may be a regular line with compacted floes, it may consist of a succession of belts or strips, or it may be frayed with off-lying isolated fragments. The ice edge is highly variable and exhibits rapid changes in ice movement and deformation (i.e., dynamical processes) and ice growth and melt (i.e., thermodynamical processes). Table 18.1 summarizes various ice edge structures. Examples of ice edge conditions found in the Arctic are presented in the chapter's images. Analysis techniques utilized to determine ice edge location and ice type near the edge are described for each SAR image.

TABLE 18.1. Ice Edge Structures [After *Ice Observation Handbook*, 1991]

Edge Structure	Characteristics						
Compacted Ice Edge	Close, clear-cut ice edge compacted by wind or current; usually on the windward side of an area of pack ice.						
Diffuse Ice Edge	Poorly defined ice edge limiting an area of dispersed ice; usually on the leeward side of an area of pack ice.						
Tongue	A projection of the ice edge up to several kilometers in length, caused by wind or current.						
Bight	An extensive crescent-shaped indentation in the ice edge, formed by either wind or current.						
Ice Field	An area of drift ice consisting of floes of any size and having an area greater than 10 km across. <table data-bbox="649 756 1266 861" style="margin-left: 40px;"> <tr> <td>Small Ice Field:</td> <td>10-15 km across</td> </tr> <tr> <td>Medium Ice Field:</td> <td>15-20 km across</td> </tr> <tr> <td>Large Ice Field:</td> <td>Greater than 20 km across</td> </tr> </table>	Small Ice Field:	10-15 km across	Medium Ice Field:	15-20 km across	Large Ice Field:	Greater than 20 km across
Small Ice Field:	10-15 km across						
Medium Ice Field:	15-20 km across						
Large Ice Field:	Greater than 20 km across						
Ice Patch	An area of drift ice less than 10 km across.						
Belt	A large feature of drift ice arrangement; longer than it is wide; from 1 km to more than 100 km in width oriented generally parallel to the main ice edge.						
Strip	Long narrow area of drift ice, about 1 km or less in width, usually composed of small fragments detached from the main mass of ice and run together under the influence of wind, swell or current.						

Variations in ice concentrations along the edge result from wind drag, tides, ocean circulation, ice ablation, or freezing and can vary on a daily, monthly, seasonal, or yearly basis. Ice edges are classified as either compacted or diffuse. Compacted edges are clearly defined due to wind and/or currents moving toward the pack. Diffuse edges are poorly defined, and are usually associated with the downwind side of the pack.

Ice edge structure type can be identified using SAR by observing the change in ice concentration within the outer ice edge region that is made up of small floes. These small floes, ranging from 20 m to 100 m in size, occur along the ice edge when processes such as ablation, freezing, and gravity-wave/ice interaction and eddy-induced collisions break up large floes. When an on-ice wind event occurs, the ice edge becomes very compact, the ice concentration approaches 100%, and the backscatter intensity values become large. When an off-ice wind event occurs, the ice edge becomes diffuse, the ice concentration reduces to values as low as 20%, and the average backscatter intensity average reduces considerably. During these events, locating the edge on SAR becomes quite easy.

Figure 18.1 is a RADARSAT-1 ScanSAR Wide (500-km swath) image of the ice edge in the Bering Sea (60.40°N, 72.27°W) collected in the winter (7 March 2000). The C-band (5.6 cm) horizontally parallel polarized image collected with a center incident angle of approximately 34.5° clearly delineates the pack ice (brighter return) from the open water that appears as dark gray in the lower one-third of the image. The exact wind speed present during the SAR

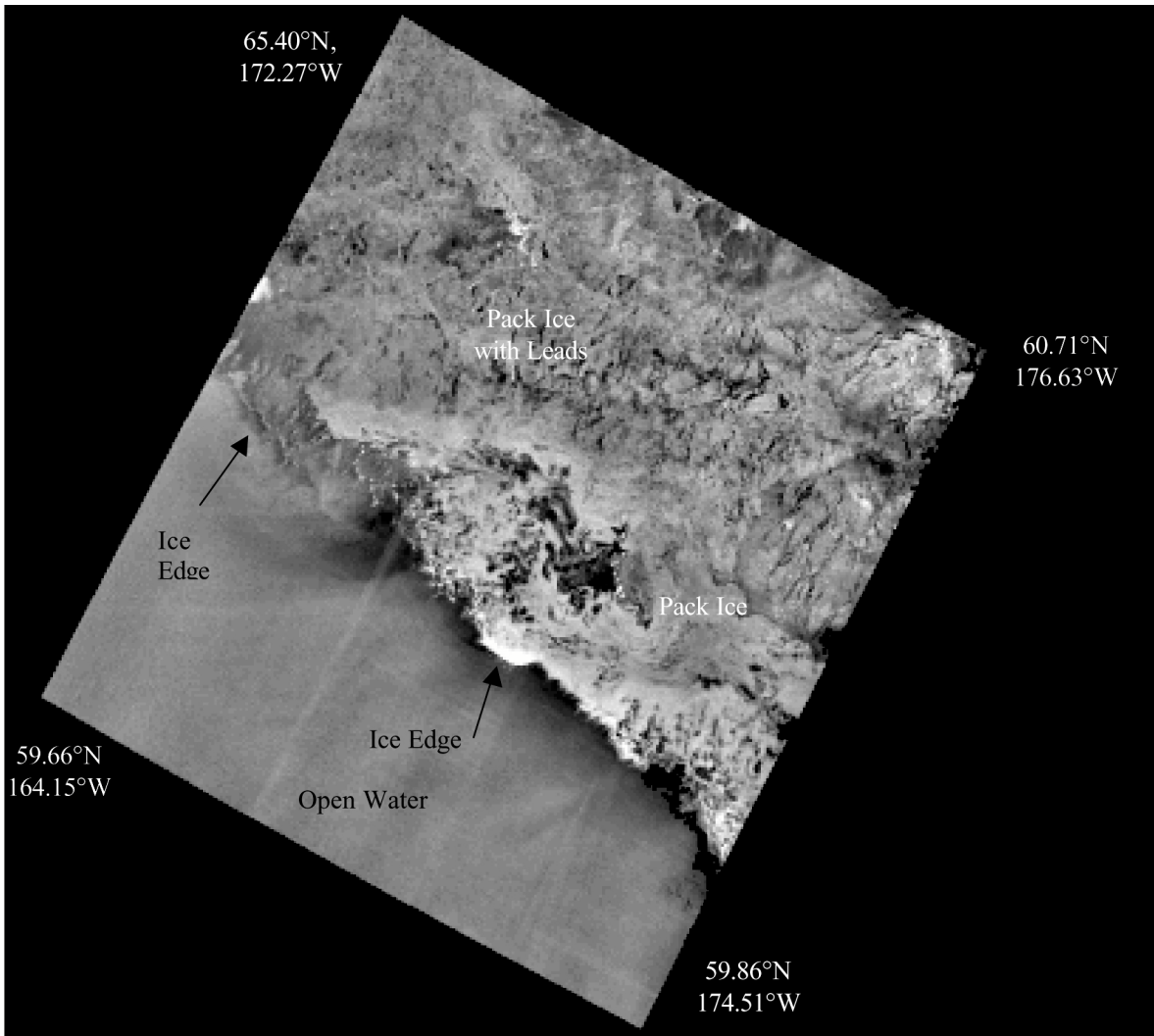


Figure 18.1. RADARSAT-1 (C-band, HH) ScanSAR Wide beam (100-meter resolution) image of the ice edge in the Bering Sea. The incident angle to the center of the image is 34.5° . The image was acquired on 2 March 2000. The ice edge is clearly delineated on the image. ©CSA 2000

collection is not known, but the backscatter suggests a wind speed of less than 7 m s^{-1} . The ice edge is compacted, further suggesting the wind was blowing from the open ocean onto the ice.

The 100-m resolution ScanSAR data provides detailed information about the ice concentration and stage of the first year ice. The bright ice at the edge is composed of pancakes that have rough edges caused by wave and wind effects. Open water leads (dark/no return areas) can be observed farther from the edge. The dark/no return right at the ice edge is mostly caused by the presence of grease ice. Grease ice dampens the ocean Bragg waves, hence no radar energy is reflected back to the satellite.

A more complex SAR image of an ice edge is shown in Figure 18.2. This scene shows some of the marginal ice zone in the Chukchi Sea in late August 1992. The pack ice lies at the bottom of the scene and the pack ice edge is located across the center. The U.S. Coast Guard icebreaker U.S.C.G. “Polar Star” was operating within the area of this scene at the time the data were obtained. The air temperature was $+5.2^\circ\text{C}$ and the wind was blowing from the east (left) at 4.1 m s^{-1} (8 knots).

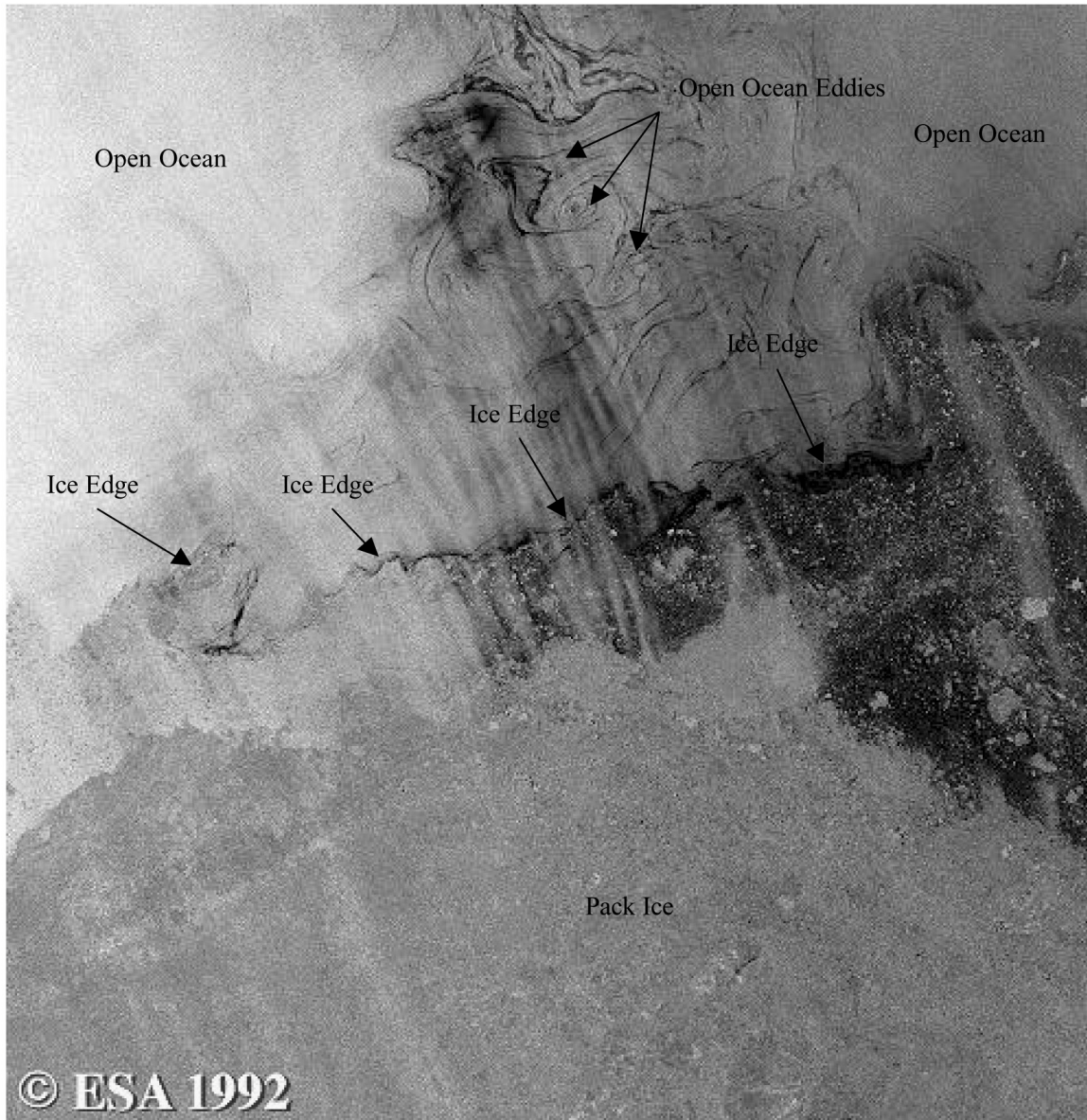


Figure 18.2. ERS-1 (C-band, VV) SAR image of the marginal ice zone in the Chukchi Sea collected on 24 August 1992. The center coordinates of the image are 72.74°N and 164.89°W. Indicated on the image are the ice edge and various ice edge features. The vertical streaks on the image are most likely caused by atmospheric internal waves. Copyright for this scene rests with ESA. This description was prepared by Martin Jeffries, Geophysical Institute and Alaska SAR Facility, University of Alaska Fairbanks, and Antony Liu, Goddard Space Flight Center.

Large-scale eddies are clearly visible in the open water area at the top of the scene. Superimposed on the eddies are long, striated wave patterns propagating from the east (left) to west (right). The long striated wave patterns, also evident in the pack ice (with ice concentration of 50% or less), are oriented perpendicular to the wind. The wind is blowing roughly parallel to the ice edge giving it a characteristic straight, tightly packed configuration.

The long wavelength (1 km to 2 km) of the striated patterns suggests that the patterns are probably the manifestation of atmospheric internal waves. Based on the ship data, the atmospheric inversion layer thickness is approximately 1.53 km with a density change of $2 \times 10^4 \text{ g cm}^{-3}$. If the striations were parallel to the wind direction, they would represent a windrow

pattern. However, the striations are almost perpendicular to the wind direction as reported from the ship. Consequently, these patterns may be caused by the low atmospheric internal waves as clear-air disturbances in a boundary layer inversion waveguide. Convergent and divergent flows induced by these internal waves will produce rougher and smoother ocean surfaces (with Bragg waves or small floes), respectively. Cloud formations associated with these disturbances are relatively rare, but they are a hazard to aviation in coastal areas.

The sea ice surface was extensively puddled at the time due to the warm air temperatures. Consequently, backscatter from the sea ice was relatively low with a narrow range (-11.4 dB). Hence the generally uniform gray tone of the ice and the poor contrast between individual, small floes. The icebreaker is not clearly visible, but can be found about 20 km (200 pixels) in from the center of the left edge of the scene where there is a small, bright feature located within a tongue at the ice edge.

The dynamics of the ice edge as imaged by SAR can be further illustrated in Figure 18.3, an area of the Greenland Sea. Each SAR strip, which is 500-km long and 100-km wide, covers the same geographical area in the ice-edge region between 76°N to 80°N, and 8°W to 4°E. This series of annotated ERS-1 images and corresponding interpretation maps shows how the ice-edge location and features changed during the period from 13 to 16 January 1992. Each of the annotated features in Figure 18.3 will be further described in this chapter. During this period, oceanographical investigations in the area were conducted from the R/V Håkon Mosby showing a number of shallow surface tongues of colder and fresher water associated with the ice tongues in Figure 18.3 [Johannessen, *et al.*, 1994].

SAR images with 25-m resolution were the only data capable of providing accurate ice-edge location in a period of almost no daylight. SAR images transmitted to the ship in near-real-time were used to route the ship to positions near the edge of the ice. Without SAR imagery, the R/V Håkon Mosby would not have been able to operate close to the edge of the ice, as the wind conditions were variable and included storm events with wind speeds exceeding 25 m s⁻¹. During southeasterly winds, the ice edge was pushed towards the west. From 10 to 13 January, the wind began as northerly and then shifted to southerly, resulting in a more eastward location of the edge. On 16 January the effects of a north-northwest wind is made visible by ice streamers in the open ocean oriented parallel to the wind. Three days later, westerly winds produced an ice edge that is very diffuse. The rapid change in edge location and detailed ice features as characteristic of this area could only be observed from a time series of SAR images. The repeat period for the ERS SAR coverage was three days.

Figure 18.3 also shows how wind speed is a determining factor in discerning the ice edge on SAR images. High wind and wave conditions will cause the open ocean to produce a large return making the intensity value similar to sea ice. The variation of backscatter with ice type and wind speed is illustrated in Figure 18.4. This figure is a C-band (5.6 GHz), VV and HH polarization backscatter (σ_0) versus radar incident angle graph for first year, multiyear, and open water at various wind speeds. The open water values were generated using an experimentally validated ocean backscatter model. The sea ice values were obtained from measurement. Special note should be given to incident angles where ERS-2 (20°), RADARSAT-1 (15°- 50°), and ENVISAT (14°- 45°) operate. Recall that ERS-2 is vertically polarized, RADARSAT-1 is HH polarized, and ENVISAT is VV, HH and cross-polarized. This figure illustrates the backscatter tone reversal for open water and sea ice backscatter that results from various wind/incident angle combinations. Furthermore, if the goal of a SAR observation is to emphasize the open water signature, SAR parameters of choice are either VV polarization, or

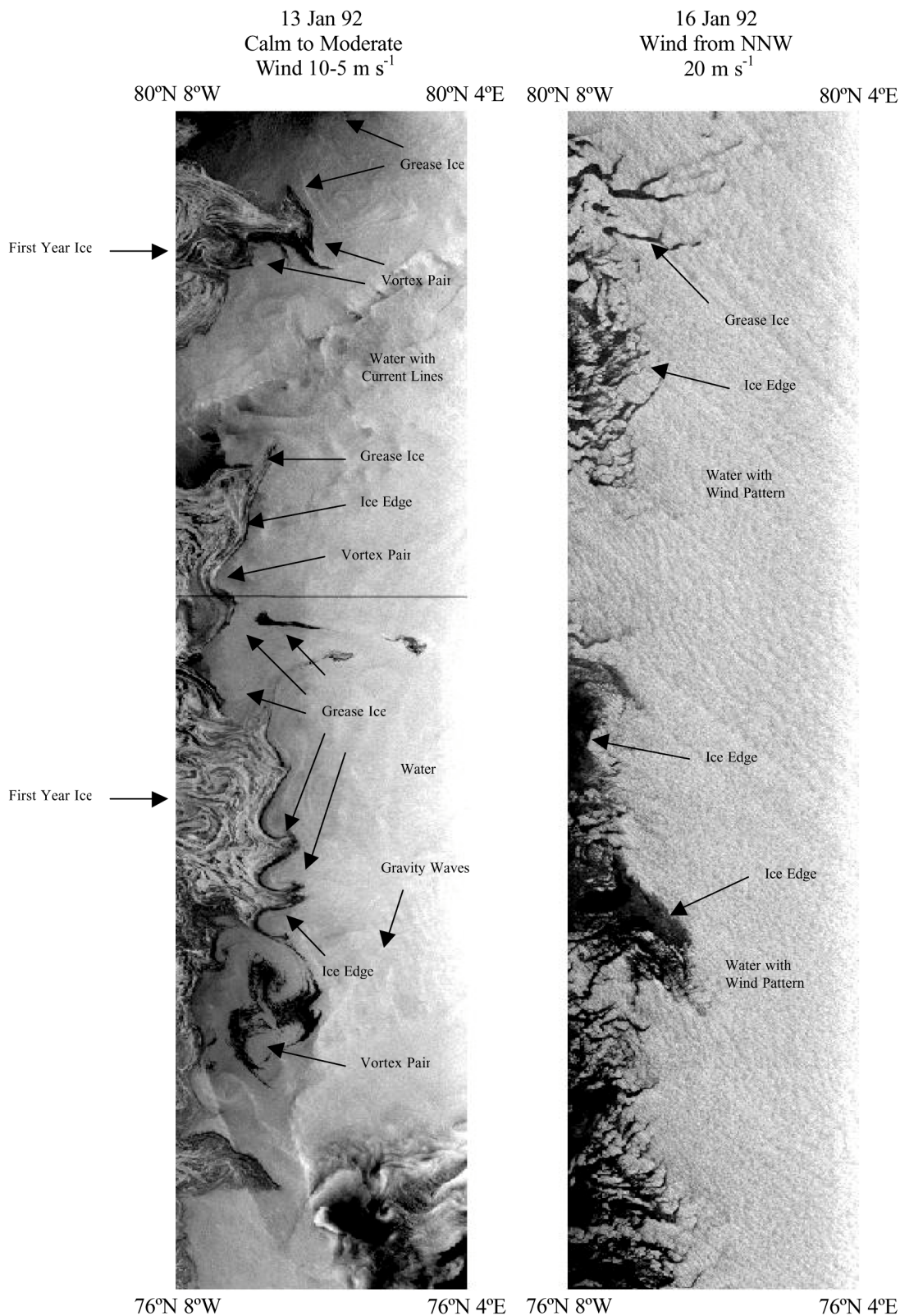


Figure 18.3. ERS-1 (C-band, VV) SAR Example of rapid ice edge variability in the Greenland Sea – Fram Strait area as a result of strong off-ice winds. The ice edge is delineated on the SAR images. Original images ©ESA 1992

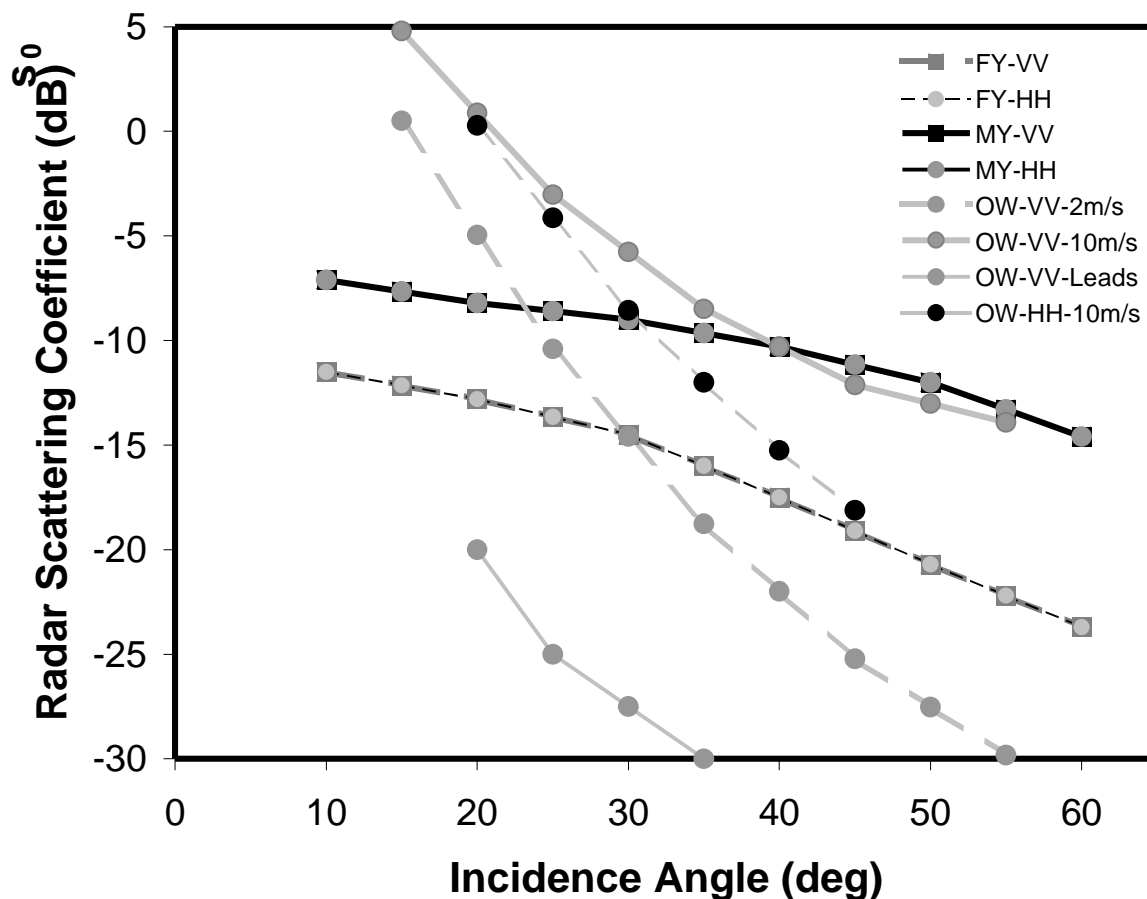


Figure 18.4. C-band backscatter versus incidence angle for first year (FY), multiyear (MY), and open water (OW) at different wind speeds. Standard deviations are ≈ 1.7 dB. The ice values are actual observation. The open water values were produced using a validated ocean backscatter model.

operating in the small to middle incidence region. If the goal is to discriminate sea ice in a liquid ocean background when winds are moderate-to-high, then HH or cross polarizations at middle-to-large angles of incidence are best.

The delineation of the ice edge on SAR imagery at the marginal ice zone in winter is complicated by the formation of new ice. As discussed by *Onstott and Shuchman* in Chapter 3 of this manual, a typical process of formation at the ice edge is as follows. Grease ice first forms followed by frazil, which then transitions into pancakes. By continued freezing and wave action, the pancakes grow from a few centimeters in diameter to meter-plus size. The SAR backscatter return from these features also varies greatly. The grease ice (see Figure 18.5) dampens the ocean wind generated Bragg waves, thus causing dark radar returns (see Figure 18.3). The pancake floes also shown in Figure 18.5 have rough edges at the water interface and, thus, are brighter SAR backscatter values on the satellite imagery.

As the ice ages and thickens at the margins, its SAR backscatter value increases (see Figure 18.4). Figure 18.6, taken from a Norwegian icebreaker at the marginal ice zone (approximately 79°N , 2°E) in March, shows snow-covered multiyear floes interspersed with fragmented first year ice. The oceanographic/meteorological buoy is being placed on a multiyear floe. The SAR return from these ice types is typically the largest ice return on the images.



Figure 18.5. Photo of Odden from the R/V Håkon Mosby showing pancake and grease ice. The pancake floes (bright circular features) are approximately 25 cm in diameter.



Figure 18.6. Photograph taken from Norwegian icebreaker at the marginal ice zone (79°N, 2°E). The buoy placement and ice sampling is occurring on a multiyear floe. Fragmented first year ice can be seen between the numerous multiyear floes shown in the photograph.

A specialized case of rapid ice formation occurs in the Norwegian/Greenland Seas and is called the Odden. The Odden is referred to in Scandinavian folk literature as a river of ice that occurs in winter during meteorological events where arctic off-ice winds have an air temperature of greater than -10°C generate rapid new ice formation (i.e., less than 24 hours). The Odden consists mainly of pancake and grease ice (see Figure 18.5), which can encompass areas in excess of 200 km x 200 km, and has been known to trap sealing ships. Figure 18.7 is an ERS-1 SAR image acquired on 16 February 1993 and cuts across the Odden ice tongue. Ice concentration obtained from the passive Special Sensor Microwave Imager (SSM/I) aboard the American Defense Meteorological Satellites on the same day as the SAR imagery agreed with the SAR-derived concentration estimates of between 20 and 30 percent [Johannessen, *et al.*, 1997a]. Note the Odden feature represents yet another form of diffuse ice edge. These types of ice were documented by observations from R/V Håkon Mosby, which operated in the northern part of the ice tongue. The ice tongue develops in December and lasts until April in some winters, but it has been absent in most years in the last decade. This absence may be related to climate change. Passive microwave data since 1978 from Scanning Multi-Channel Microwave Radiometer (SMMR) and SSM/I show that the ice tongue is absent during some winters, as was the case in 1994, 1995 and 1996 [see Shuchman, *et al.*, 1996]. Note Jan Mayen Island located at the bottom of the image. Figure 18.7 further illustrates that fine resolution SAR satellite data can not only locate the ice edge, but also discriminate the ice components that comprise the marginal ice zone.

18.3 Detection of Ice Edge Eddies and Open Ocean Phenomena Associated with the Pack

The general characteristics of ice edge conditions as seen in SAR imagery and discussed in the preceding sections can be used to identify and interpret a variety of ice edge phenomena such as ice and open water eddies. A number of these phenomena are summarized in Table 18.2. The following text describes steps involved in the use of SAR imagery to detect ice edge eddies and other features of the marginal ice zone.

Ice edge eddies in the Greenland Sea and Fram Strait area were investigated for the first time during the MIZEX program using remote sensing in combination with in-situ observations [O.M. Johannessen, *et al.*, 1987, J.A. Johannessen, *et al.*, 1987]. The ice edge eddies, a result of warm and cold ocean water masses interacting, are important for several reasons, i.e., as a mechanism to exchange heat and mass between open water and ice covered regions, in controlling the position of the ice edge, and to advect water masses trapped in the eddies. Mesoscale eddies, which have a typical scale of 20 km to 40 km in the Greenland Sea area, can also elevate intermediate water masses to the surface and contribute to deep-water formation [O.M. Johannessen, *et al.*, 1991]; hence, they are important to the oceanic uptake of atmospheric carbon dioxide and other climatic gases. Eddies are also an area of typically higher than normal ambient acoustic noise due to ice floe collisions.

Eddies are most readily observed along the ice edges where SAR images show a sharp contrast between ice and water. SAR can be used to locate eddies along ice edges because individual ice floes act as tracers mirroring the ocean circulation [Sandven, *et al.*, 1991, and J.A. Johannessen, *et al.*, 1987]. When eddies occur within the ice pack, they are much more difficult to detect in the SAR images. In regions of open water, it is necessary to use infrared or visible imagery to look for sea surface temperature gradients or color contrast to locate vortex-pairs.

Extensive remote sensing studies of the marginal ice zone in the Greenland/Iceland/Norwegian Sea have been conducted by the Nansen Environmental and,

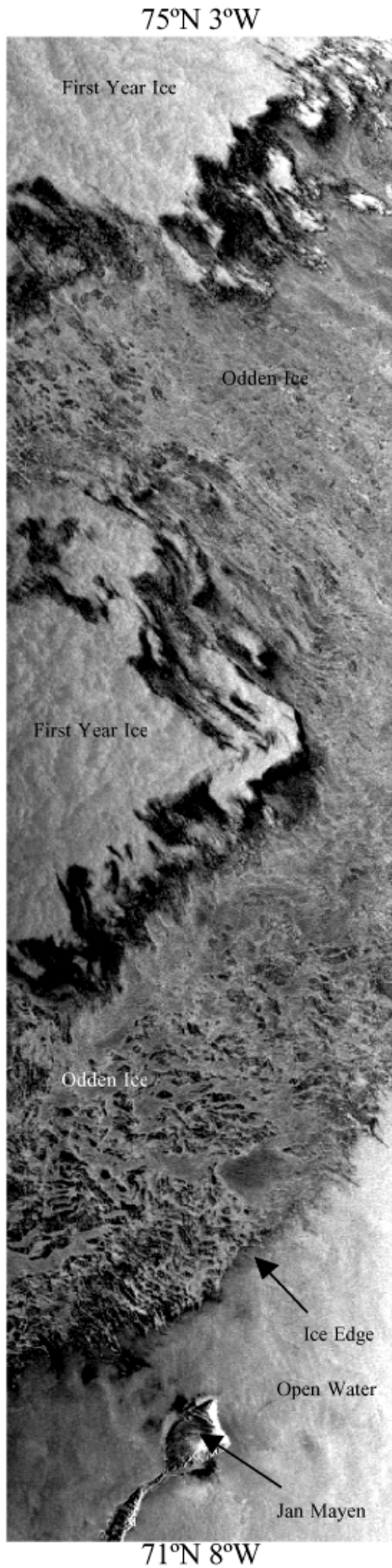


Figure 18.7. ERS-1 (C-band, VV) SAR image (16 February 1993) of Odden ice tongue. Jan Mayen Island is at image bottom. Note the delineation of the ice edge on the SAR image. Original image ©ESA 1993

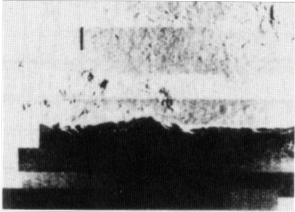
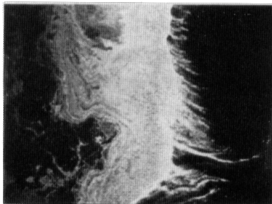
Remote Sensing Center and its partners during the MIZEX and SIZEX programs [Johannessen, *et al.*, 1992]. Based on SAR aircraft and satellite images obtained during the campaigns since 1979, a conceptual SAR model for the marginal ice zone has been formulated to identify the different ice edge processes (Table 18.2). In this scheme, the ice edge configurations from SAR images have been classified and related to atmospheric and oceanic conditions [J.A. Johannessen, *et al.*, 1991]. This conceptual SAR model provides useful guidelines for further numerical modeling of the marginal ice zone. Furthermore, a realistic ice model must be coupled to the ocean, both dynamically and thermodynamically.

A fine resolution L-band SAR mosaic collected from the CCRS CV-580 X-, C- and L-band airborne system on 5 July 1984 (Figure 18.8) clearly shows detailed surface structure of an elliptically shaped eddy (E1 in Figure 18.8b) on a scale of approximately 30 km. Also included in the figure is an oblique aerial photograph taken of this eddy from the CV-580. Because winds were light, the sea ice floe-size distribution of 50 m to 500 m reflected the upper ocean circulation. The three-dimensional structure of the eddy, as obtained from conductivity, temperature, density (CTD) section, is also shown on the figure. The orbital motion of the eddy was cyclonic, while the spiral motion of ice toward the center indicated an inward frictionally driven radial motion. The ice concentration was more than 80% at the center of the eddy. This implied that there was convergence, and that ageostrophic effects are important and must be included in realistic models of these eddies [Shuchman, *et al.*, 1987, and J.A. Johannessen, *et al.*, 1987]. Slicks and bands of ice were also identified that indicated internal wave activity. In Figure 18.8b, the area marked “band of dead water” off the ice edge was a distinct meltwater zone. This detailed interpretation of the SAR mosaic describes the location of large individual floes, polynyas, ice concentration estimates, the ice edge and floe size distributions [see Shuchman, *et al.*, 1987, and O.M. Johannessen, *et al.*, 1987].

Note in Figure 18.8 that the compacted summer ice edge is easily discerned from open water. In addition, the L-band (HH) image collected during Marginal Ice Zone Experiment (MIZEX) '84 clearly shows the large multiyear floes (upper portion of Figure 18.8a), which can be identified by their distinct outline, the ridging that occurs within the floe, and the weak SAR signature typical of a multiyear floe during the summer season. The brightness of the multiyear SAR return decreases during the summer melt season because of the high loss associated with the free water within the snow cover and the pooling of water on the surface. Since liquid water prevents significant microwave penetration, the volume scattering, which distinguishes various ice types during the winter freeze, is not present [Shuchman, 1990]. The mosaic also further demonstrates the utility of the SAR to retrieve varying floe size, slicks, and internal wave information.

The monitoring of deep water convection using SAR has also been reported [Carsey and Garwood, 1993]. Deep water convection, the mixing process that transforms warmer surface water into colder deep water, is the key first step in the global thermocline circulation and is an important process often linked with the location of the sea ice edge. Over 90% of the deep water formation in the northern hemisphere occurs in the Labrador and Greenland/Norwegian Seas. The frequency and extent of the deep water formation is an important global change question. The geographic remoteness and temporal variability of deep ocean convection has led to the consideration of using satellite remote sensing to study the convective process. Remote sensing is complimentary to in-situ oceanographic sampling and offers an additional way to obtain information on the two-dimensional horizontal extent and structure of a region of open ocean undergoing convection.

TABLE 18.2 Conceptual SAR Model for the Marginal Ice Zone [After Johannessen *et al.* 1992]

SAR Image Example	SAR Ice Edge Configuration	Ice Edge Process	Atmospheric Conditions	Upper Ocean Conditions
	Straight	Upwelling	Parallel Strong to Moderate Wind	Along Ice Jet and Divergent Ekman Flow and Convection
	Meandering and Eddies	Ice-Ocean Eddies	Moderate to Calm Wind	Ocean Eddies, Precondition, Convection
	Ice Jet Perpendicular to the Edge	Momentum Pulse, Ice Jet, and Vortex-Pair	Moderate to Calm Wind	Shallow Upper-Layer Ocean Jet
	Low Backscatter off the Ice Edge and in Leads	Ice Freezing (Winter) Ice Melting (Summer)	Calm or Off-Ice Wind Sun Radiation	Salinity and Density Increase, Convection Fresh Water, Increased Stratification
	Wave Pattern and Compact Small Floes	Wave Propagation, Refraction, and Attenuation	On-Ice Wind	Wind Waves and Swell Propagating Towards the Ice
	Ice Banding, Streamers, and Internal Waves	Ice Bands and Internal Waves	Off-Ice Wind or Varying Wind	Convergence, Divergence, Internal Waves

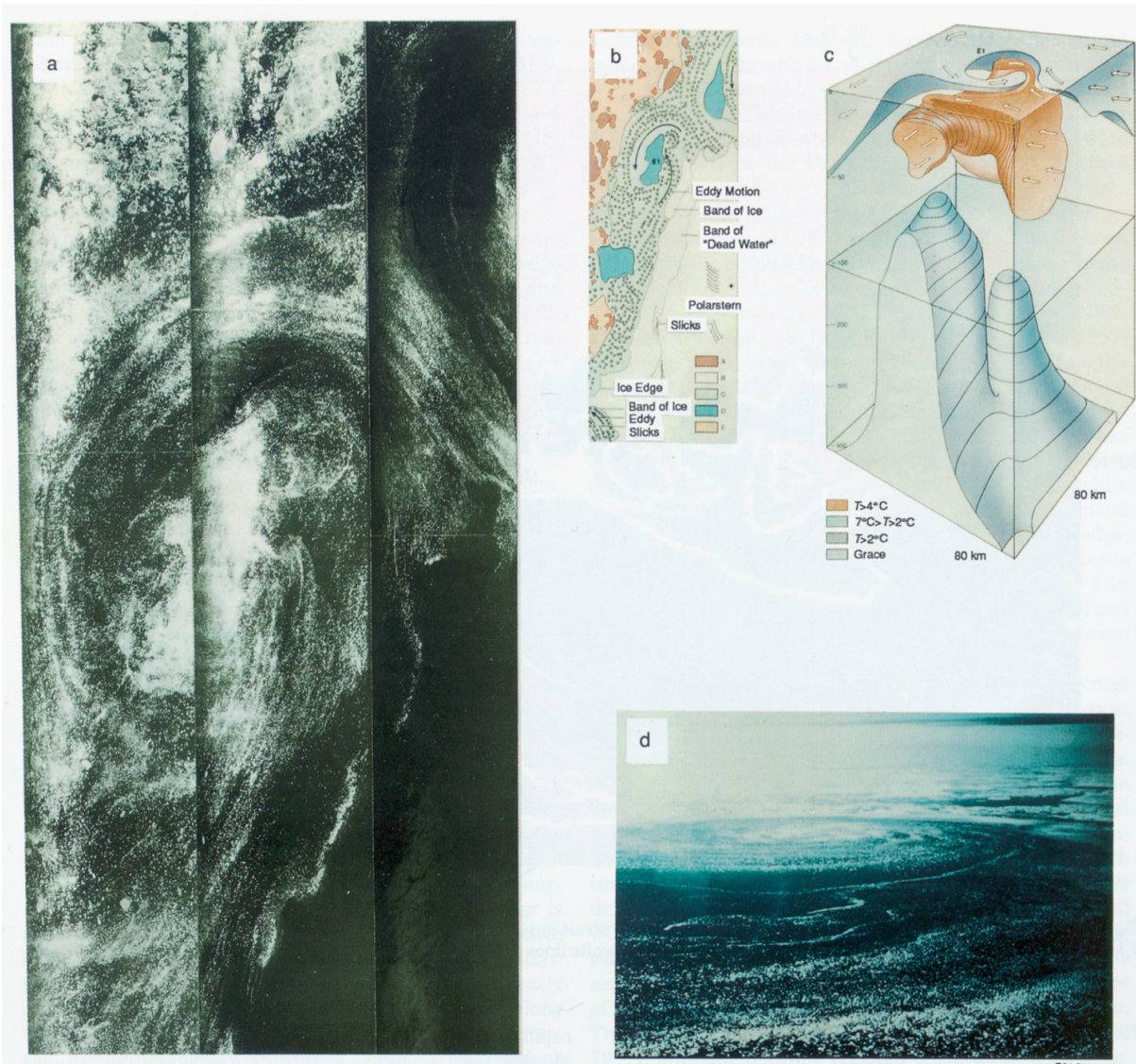


Figure 18.8. (a) CCRS CV-580 aircraft SAR (L-Band, HH) image acquired on 5 July 1984, of a cyclonic ice edge eddy in the Greenland Sea, (b) interpretation of the whole SAR mosaic, (c) three-dimensional structure of the eddy obtained from conductivity, temperature, density (CTD) sections, (d) oblique aerial photograph of the eddy [After Johannessen, *et al.*, 1992]. This eddy was located at approximately 78°50' N and 2°30' W. Large multiyear floes can be seen in the upper left portion of the SAR mosaic.

Figure 18.9 is a 12 March 1997 ERS-2 SAR image taken in the Labrador Sea in a region where in-situ observations reported deep water convection. Deep water convection cells, sometimes referred to as chimneys [Fisher, *et al.*, 2000], are identified and outlined in the figure.

18.4 Waves in the Pack Ice

SAR has been shown to be capable of detecting ocean wind waves and swell within the sea ice cover at the marginal ice zone when it is comprised of ice floes tens of meters in diameter. Observations to date have been made using airborne CV-580 X- and L- band [Lyzenga, *et al.*, 1985] and CV-580 C-band [Liu, *et al.*, 1991a, 1991b] SAR data as well as using space borne ERS-1-2 and RADARSAT-1 data [Johannessen, *et al.*, 1997a].

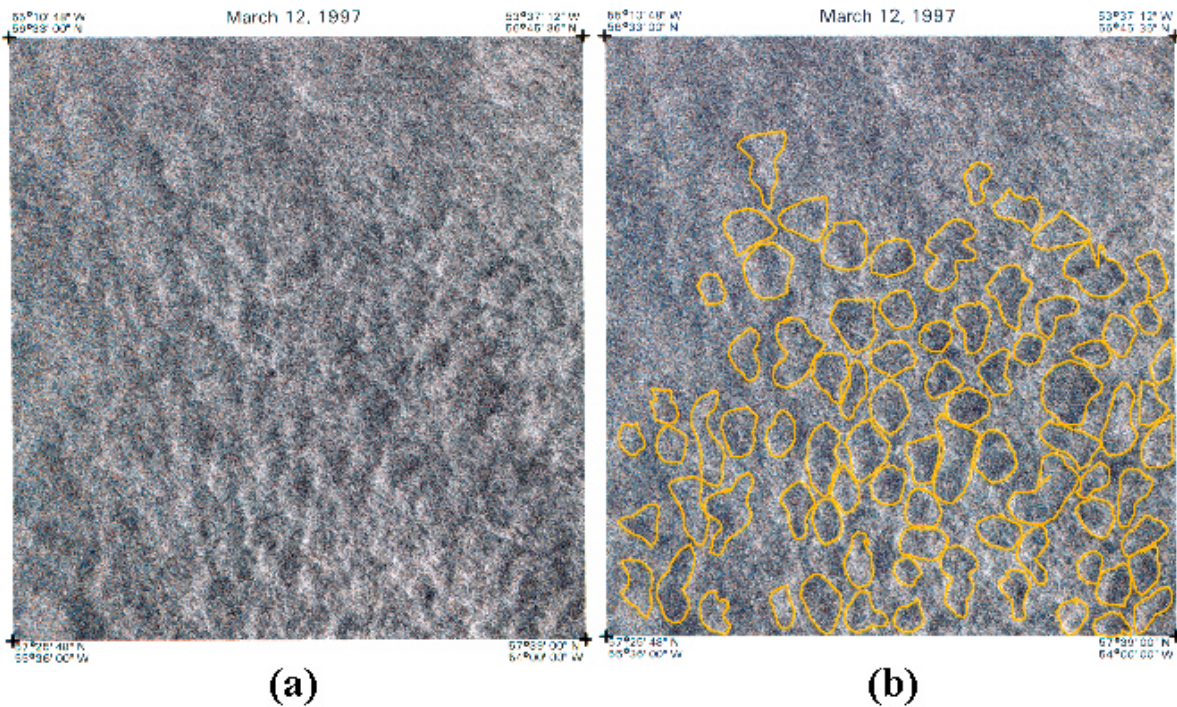


Figure 18.9. Manual analysis of ERS-1 (C-band, VV) image showing deep water formation cells.
Original image ©ESA 1997

The complex mesoscale air-sea-ice interactions in the marginal ice zones are enhanced by open ocean waves that penetrate into the ice cover. Penetrating waves contribute to the breakup of floes, increase in melt rate, and variation in ice concentration and ice extent. Simultaneously, the ice imparts resistance to the waves, which alters the wave dispersion properties and results in a reduction or attenuation of wave amplitude. The imaging of wave propagation into the ice is also important from a navigation, acoustic noise, and offshore petroleum exploration perspective. All of these interactions are dependent on wave period, wave height, ice thickness, floe size, and concentration. Waves may be apparent in an ice cover for considerable distances from the ice edge (e.g., propagation up to 100 km have been observed). For example, Figure 18.10 presents multiple channels of airborne SAR imagery of ocean waves propagating approximately 60 km into pack ice off of the Labrador coast. A detailed overview of the characteristics of waves in ice is found in *Wadhams* [1986].

When waves propagate into an ice cover, attenuation of the wave amplitude and alteration of the wave dispersion properties occurs. As a wave penetrates into a uniform, large ice sheet, the wave energy is transmitted and shared between the ocean and ice, resulting in what is known as a flexural-gravity wave. For long period waves or for thin ice, waves have lengths, and phase and group velocities similar to those of open water. As the ice thickens for a given wave period, the wavelength, phase, and group velocities will increase over those for the open water case. These changes increase with decreasing wave period. Similarly, wave amplitude decreases with increasing ice thickness and decreasing wave periods, with very long waves retaining amplitudes in ice similar to those of open water.

The observation of refraction and attenuation of gravity waves as they propagate into the ice has been studied in both the Arctic and Antarctic. *Shuchman, et al.* [1994] demonstrated that ice thickness could be obtained by observing gravity propagation into the ice. A study by

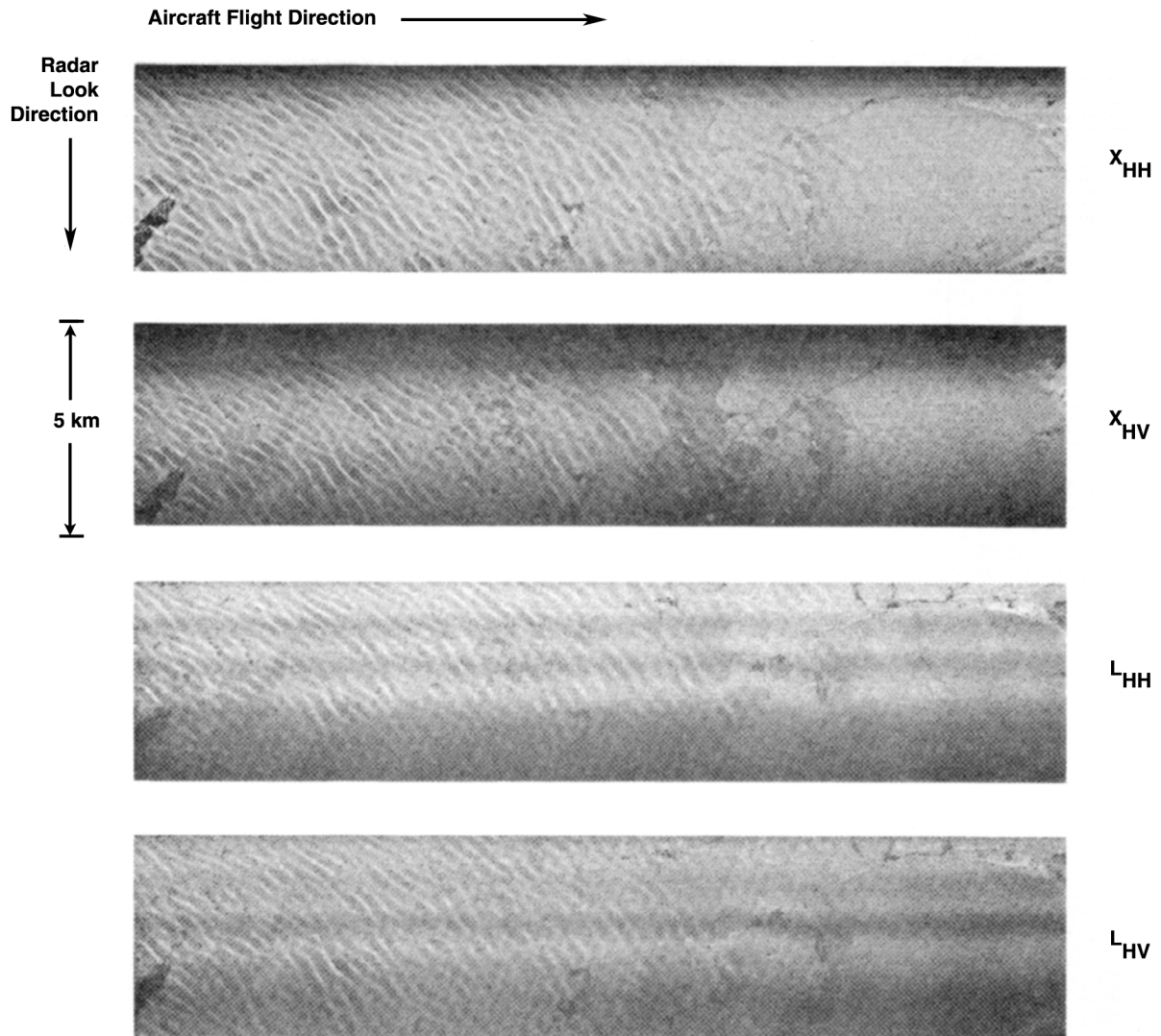


Figure 18.10. Multiple channels of airborne SAR imagery of ocean waves propagating approximately 60 km into pack ice off the Labrador coast near Hopedale.

Wadhams and Holt [1991] suggests that gravity waves propagating through Antarctic pancake and frazil ice can also be imaged by SAR, and the SAR data (by observing attenuation of the gravity waves) can then be used to extract the thickness of these two ice types. This thickness information could then be used to better determine the advancing winter ice edge in the Antarctic.

18.5 Examples from the Kara Sea Northern Sea Route

Since the launch of the ERS-1 satellite in July 1991, the Nansen Environmental and Remote Sensing Centers in Bergen and St. Petersburg, in cooperation with the European Space Agency and Murmansk Shipping Company, have demonstrated the capability of SAR images with resolution of about 100 m x 100 m to provide detailed sea ice information of the Russian Northern Sea Route. From SAR images, most of the important sea ice parameters such as edge, type, concentration, motion and surface roughness can be extracted [*Johannessen, et al., 1997b*].

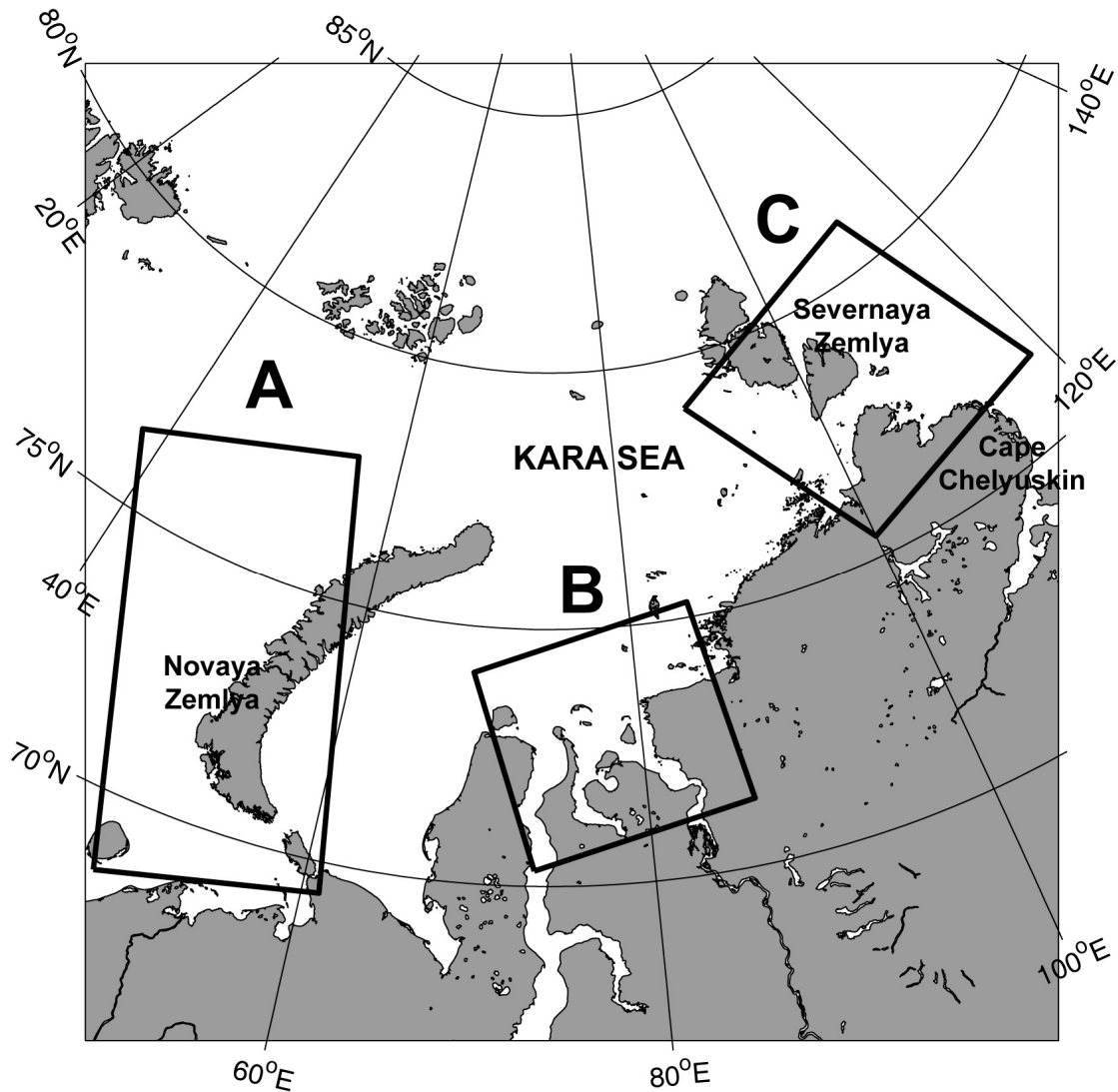


Figure 18.11. Map of the western Russian Arctic with boxes showing the coverage of the three images presented in this section: (A) covers the eastern Barents Sea and the southern part of Novaya Zemlya, (B) covers the central Kara Sea where the Ob and Yenisei rivers enter the Arctic Ocean, and (C) covers the Vilkitsky Strait area where Cape Chelyuskin represents the northernmost landfast point of the Eurasian continent.

Despite the relatively narrow swath of 100 km, ERS SAR data has proven to be useful for mapping small ice areas, in particular straits, river estuaries and first year ice among multiyear ice floes. During the ERS demonstration expeditions with Murmansk Shipping Company's icebreakers, it was shown that appropriately processed SAR images with superimposed coastline and geographical coordinates are useful for strategic, as well as tactical, ice navigation [Johannessen, *et al.*, 1997b]. Since 1996, RADARSAT-1 ScanSAR images with swath width up to 500 km have been used to map large sea ice areas.

In this section we present some examples of SAR ice observations in the western Russian Arctic. The first example is from the eastern Barents Sea and Novaya Zemlya area, the second is from the central Kara Sea where the Ob and Yenisei rivers enter the Arctic Ocean, and the third is from the Vilkitsky Strait area (Figure 18.11).

Processes at the Ice Edge – The Arctic

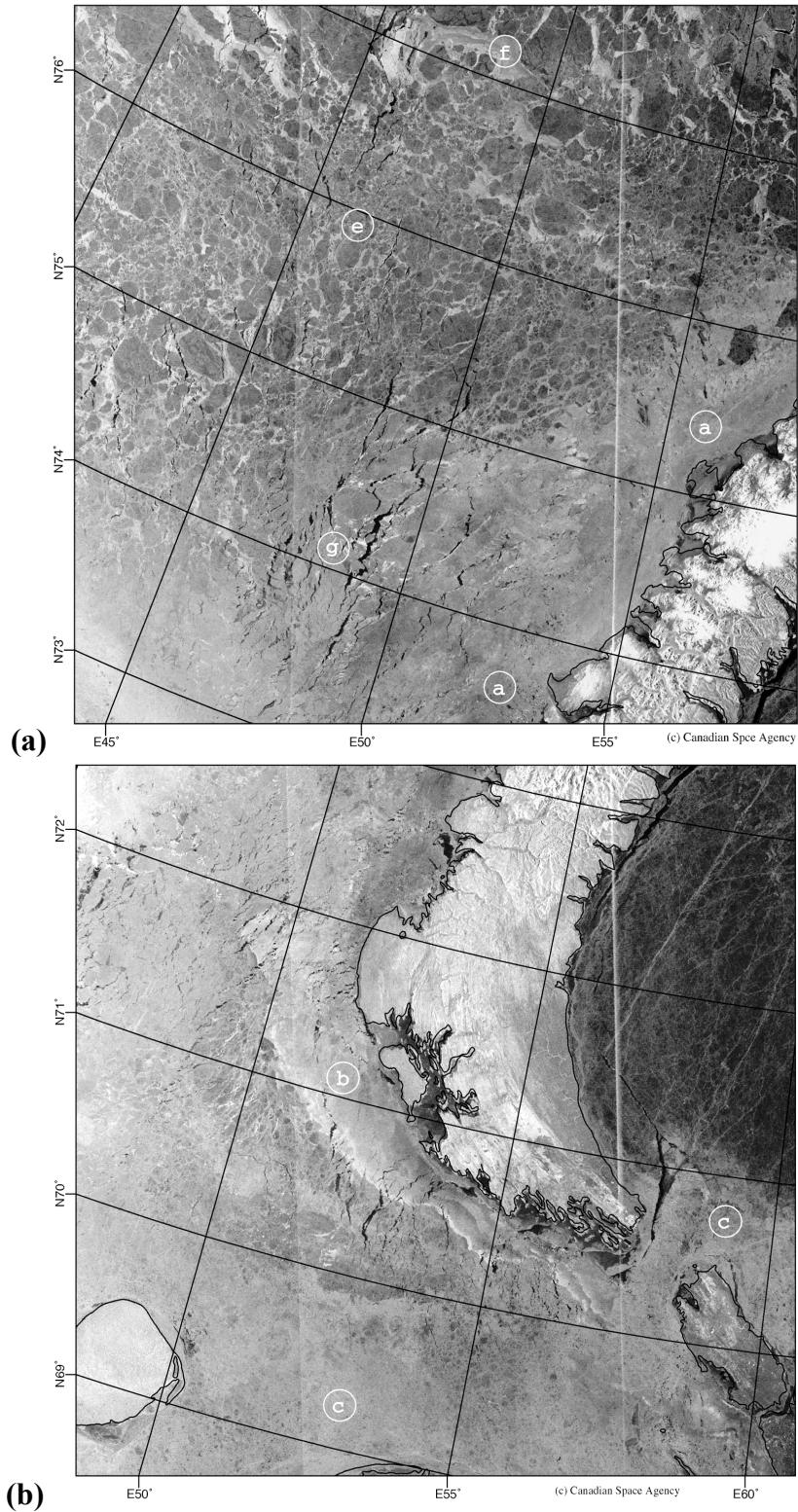


Figure 18.12. RADARSAT-1 (C-band, HH) ScanSAR images (500 km x 500 km) obtained from the same orbit on 23 April 1998, covering (a) the northeastern Barents Sea, and (b) the southeastern Barents Sea including the Pechora Sea and the Kara Gate region. The main ice features, denoted a - f, are described in Section 18.5.1 [Alexandrov, *et al.*, 2000]. Original image ©CSA 1998

18.5.1 Eastern Barents Sea and Novaya Zemlya Area

The Kara Gate and Jugor Strait are important sailing passages of the Northern Sea Route where ice can cause severe difficulties, especially in combination with strong currents. During the winter these straits can be blocked by heavy, deformed and compressed first year ice floes more than four meters thick.

Two consecutive RADARSAT-1 ScanSAR scenes obtained on 23 April 1998 show examples of ice conditions in the ice edge region of the eastern Barents Sea (Figure 18.12). The images were used to support ice navigation of an ice-going tanker going from Murmansk to Ob Gulf [Pettersson, *et al.*, 1999, Alexandrov, *et al.*, 2000].

The image shows that Kara Gate had severe ice, while the ice conditions along the western shores of Novaya Zemlya were much easier for ice navigation. For this reason the eastbound expedition with the ice-going tanker escorted by Russian nuclear icebreakers selected a route north of Novaya Zemlya.

The ScanSAR images (Figure 18.12) showed the gray-white ice of the coastal polynya on the western side of Novaya Zemlya as brighter signatures labeled (a) in the upper image compared to the thicker first year ice farther north and west. A southward extension of the polynya into the Pechora Sea and towards the Kara gate is also identified in the lower images as a bright feature (b). Rough first year ice with a bright signature dominates in the Pechora Sea, and a tongue of this ice is extending through the Kara Gate and into the Kara Sea (c). The contrast between this rough and more level first year ice east of the Kara Gate is noteworthy. The bright line structures east of Novaya Zemlya are major ridges visible because of the contrast to the level ice. Level first year ice is also observed as large dark floes north of about 75°N (e). The bright areas between the first year floes in this region are young ice (f). Between 73°N and 75°N, small leads of open water, oriented nearly in a north-south direction, are clearly seen as dark stripes in the image (g).

18.5.2 Polynyas and Landfast Ice in Ob and Yenisei Area

As the tanker expedition continued into the Kara Sea towards the Ob Gulf, another RADARSAT-1 ScanSAR image was obtained (Figure 18.13). This image demonstrates late winter ice conditions in the Kara Sea from the Ob estuary in the west to the shores of Taymyr in the east, with temperature between -10°C to -15°C and winds of about 10 m s⁻¹ from NE. The image has a complex pattern of ice types, and several areas are difficult to interpret with certainty. Large areas with landfast ice are seen with a gray signature off the coasts and around the islands. In these areas the backscatter varies considerably and depends on the salinity, ice age and roughness. In general, strong backscatter indicates that the ice has a low salinity and rough surface. The image interpretation could be done by use of in-situ observations from the expedition.

The image can roughly be divided into three regions: medium and thick first year ice in the upper part of the image (1 and 2), polynya areas with various types of new and young ice including open water (3, 4 and 5), and finally the landfast ice regions near the coast and the islands (6 and 7). Area (1) consists mainly of large thick first year ice floes (darker), with smaller areas with young ice (brighter) and nilas (very dark) in-between. Some of the darker small areas might also be water. Some areas have strongly deformed thin and medium-thick first year ice (2), with some inclusions of young ice (light gray). The very bright parts of the polynya area (3) consists of deformed young ice, while areas (4) and (5) are most likely a mixture of

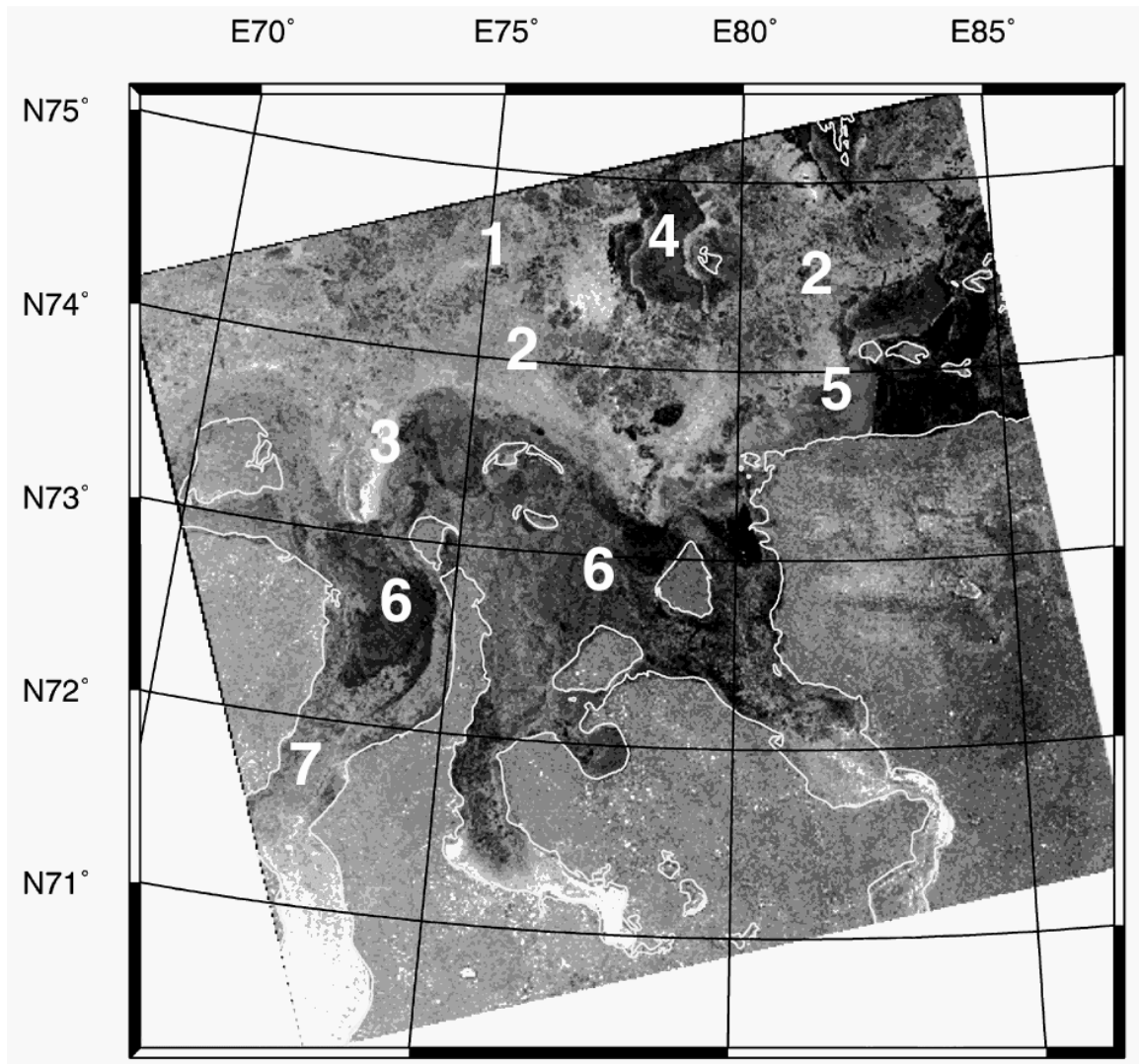


Figure 18.13. RADARSAT-1 (C-band, HH) ScanSAR image of 30 April 1998, covering area where the Ob and Yenisei rivers enter the Kara Sea. The ice types 1-7 are discussed in the text. Original image ©CSA 1998.

water and thin ice types such as grease ice and nilas. Areas (6) and (7) show landfast ice of various age and deformation. The darker signature indicates the more level and undeformed ice, while greater backscatter (lighter tone) suggests more roughness. Roughness at the surface, seen in the ice deep into estuaries, may be due to a lower salinity of river water. It is assumed that the high backscatter in the inner parts of the bays is a combined effect of roughness and volume scattering from the freshwater ice created in the river estuaries.

18.5.3 The Vilkitsky Strait and Surrounding Areas

The Vilkitsky Strait is the northernmost part of the Northern Sea Route, located between the Kara Sea and the Laptev Sea (Figure 18.14). This strait is particularly difficult to navigate when ice covered, navigation is only attempted during the summer season. Thick residual floes (second- or multiyear ice) often occur in this region where differential ice motion causes heavy compression and ridging of the ice pack. The large thick floes, heavy ridges, and landfast ice makes it difficult to navigate even for the most powerful icebreakers.

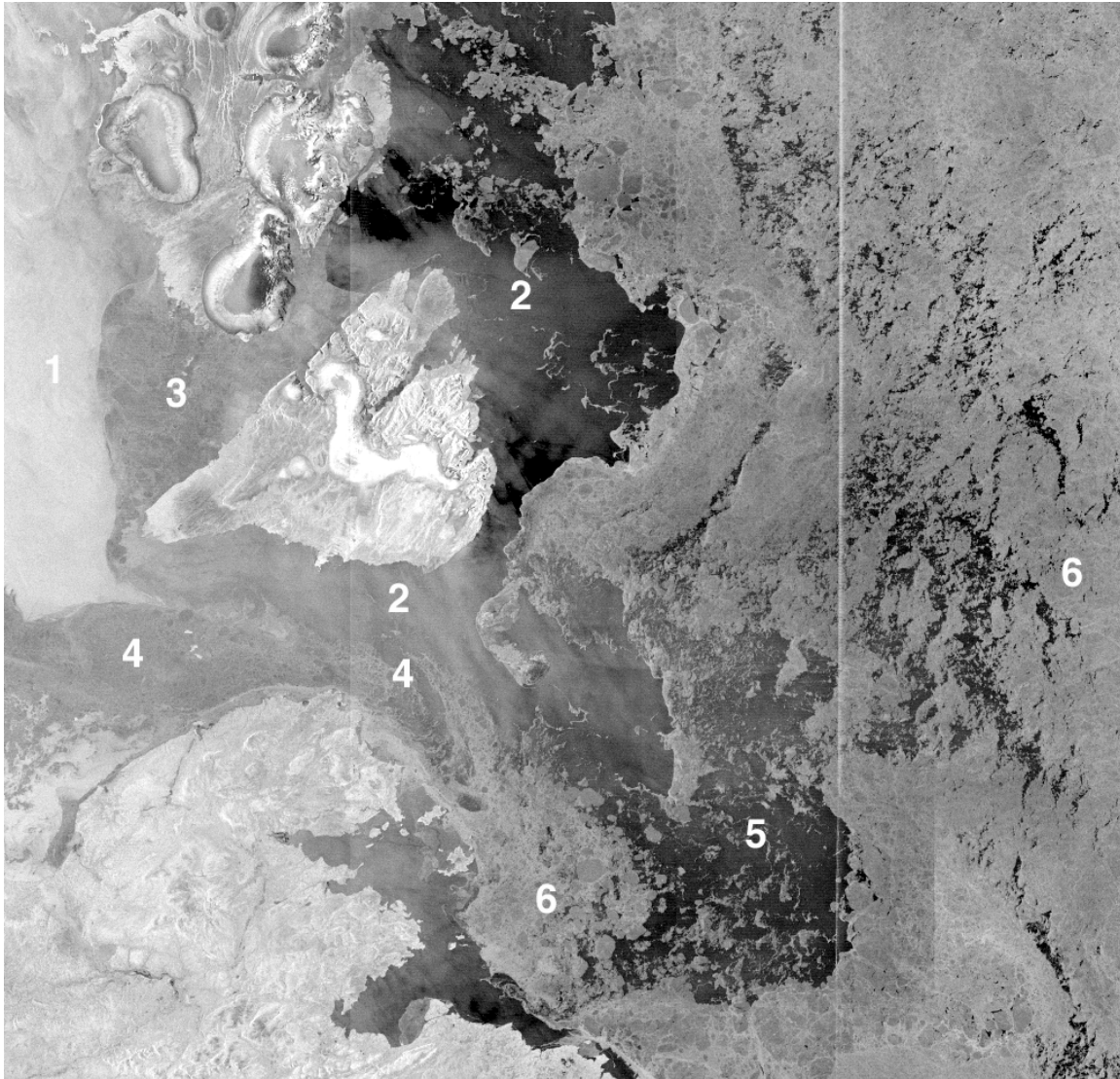


Figure 18.14. RADARSAT-1 (C-band, HH) ScanSAR image from 14 August 1997, covering the eastern Kara Sea, the Vilkitsky Strait and the western part of the Laptev Sea. The ice types 1-6 identified on the figure are discussed in the text. The center coordinates of this image are approximately 78°N and 105°E. Original image ©CSA 1997

The image in Figure 18.14 was taken during an expedition with the Russian nuclear icebreaker “Sovetsky Soyuz” during its voyage to the Laptev Sea in August – September 1997 [Sandven, *et al.*, 2001]. The ice conditions were typical in a melting stage with air temperatures above 0°C and moderate-to-low wind speeds. Observations onboard the icebreaker were used to interpret the SAR signatures. Open water dominates the Kara Sea with bright signatures caused by 6-8 ms⁻¹ winds (1). Parts of the Vilkitsky Strait and Laptev Sea are open water with dark signature as a result of lower winds and mixed with stripes and patches of first year ice from the previous winter (2). The landfast ice in the Shokalskogo Strait (3) is melting and breaking up, and some ice will drift into the currents of the Vilkitsky Strait, that transport remnants of first year ice from the Kara Sea to the Laptev Sea (4). This transport forms a characteristic wedge penetrating into the thicker and more compact first year ice in the Laptev Sea. This ice is called the Taimyr Ice Massif and consists mainly of first year ice from the previous winter (6).

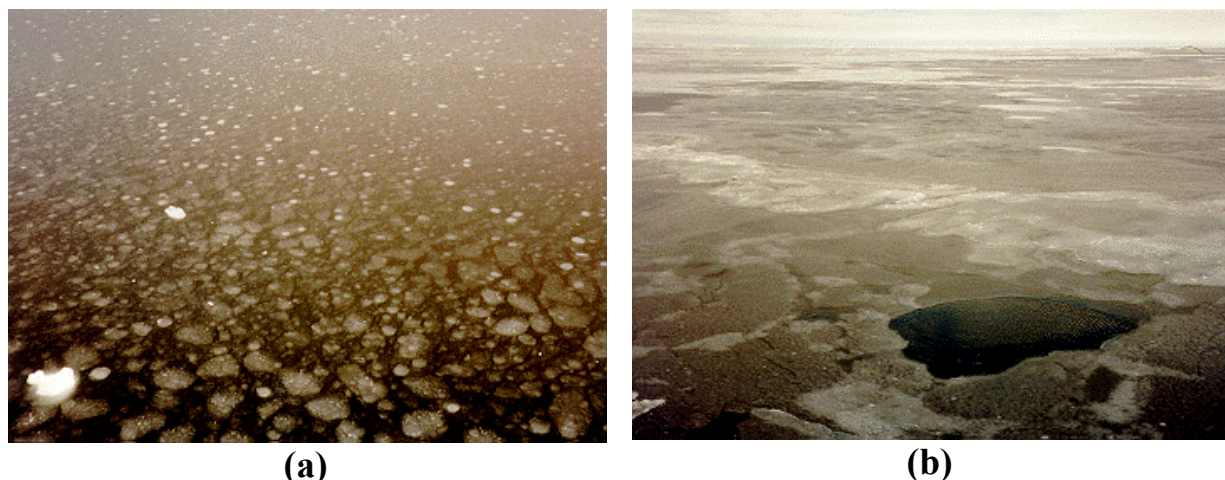


Figure 18.15. Photographs of pancake ice (a) and nilas (b) obtained in the Vilkitsky Strait area on 10-11 September 1997, about four weeks after the ScanSAR image in Figure 18.14 was obtained. Picture (a) was taken at 77°55'N 104°20'E, picture (b) was taken at 77°38'N 111°01'E.

This ice massif is partly breaking up as a result of the eastward transport of more open water through the Vilkitsky Strait (5). The ice conditions shown in Figure 18.14 represent typical minimum ice extent at the end of the melt season in this area. During the next month air temperature stayed at about -5°C , allowing new ice to be formed. Examples of grease ice and nilas in the Vilkitsky Strait area are shown in pictures taken from an icebreaker sailing through the area on 10-11 September 1997 (Figure 18.15).

18.6 Summary

This chapter has demonstrated the utility of SAR data to characterize ice edges. SAR is well suited to discriminate ice from open water when the effect of wind speed is taken into account. Often in lower wind conditions (less than 7 m s^{-1}) the ice will mirror the surface ocean circulation and various eddies, fronts, internal waves and particularly deep water convection cells (chimneys) can be observed. The fine resolution (25 m) of SAR compared to spaceborne passive microwaves systems with maximum resolution of approximately 10 km makes SAR imagery particularly useful in studying small-scale features at the ice edge. These features include areas of grease ice, pancake floe, first year and multiyear floes, and polynyas. Observation of gravity waves propagating into the pack is also possible due to the fine resolution imaging capability. In addition to providing detailed information on sea ice and ice/ocean processes, the level of image detail in SAR data is useful for mapping ice conditions important to navigation, as illustrated by the sequence of images along the Northern Sea Route.

18.7 References

- Alexandrov, V. Y., S. Sandven, O. M. Johannessen, Ø. Dalen and L. H. Pettersson, 2000: Winter navigation in the Northern Sea Route. *Polar Record*, **36**, 333–342.
- Carsey, F. D., and R. W. Garwood Jr., 1993: Identification of modeled planes in Greenland Gyre ERS-1 SAR data. *Geophys. Res. Lett.*, **20**, 2207–2210.
- Fisher, K. W., C. A. Russel, R. A. Shuchman, and J. Johannessen, 2000: Deep ocean convection observed by ERS-2 SAR and in situ data in the Labrador Sea. (Unpublished)

- Ice Observation Handbook, 1991: Prepared by: Commanding Officer, Naval Polar Oceanography Center, 4301 Suitland Rd Washington, DC 20395-5180, 118 pp.
- Johannessen, J. A., and Coauthors, 1987: Mesoscale eddies in the Fram Strait marginal ice zone during the 1983 and 1984 Marginal Ice Zone Experiment. *J. Geophys. Res.*, **92**, 6754–6772.
- , and Coauthors, 1991: NORCSEX'91 science and operation plan. Nansen Remote Sensing Center, Bergen, Norway, 55 pp.
- Johannessen, O. M., J. A. Johannessen, E. Svendsen, R. A. Shuchman, W. J. Campbell, E. G. Josberger, 1987: Ice-edge eddies in the Fram Strait marginal ice zone. *Science*, **236**, 427–429.
- , S. Sandven, and J. A. Johannessen, 1991: Eddy-related winter convection in the Boreas Basin. *Deep Convection and Deep Water Formation in the Oceans*, P. C. Chu and J. C. Gascard, Eds., Elsevier Oceanography Series, Vol. 57, Elsevier, 87–105.
- , W. J. Campbell, R. A. Shuchman, S. Sandven, P. Gloersen, J. A. Johannessen, E. G. Josberger, and P. M. Haugan, 1992: Microwave study programs of air-ice-ocean interactive processes in the seasonal ice zone of the Greenland and Barents seas. *Microwave Remote Sensing of Sea Ice, Geophys. Monogr.*, No. 68, Amer. Geophys. Union, 261–289.
- , S. Sandven, W. P. Budgell, J. A. Johannessen, and R. A. Shuchman, 1994: Observation and simulation of ice tongues and vortex-pairs in the marginal ice zone. *The Polar Oceans and their Role in Shaping the Global Environment, Geophys. Monogr.*, No. 85, Amer. Geophys. Union, 109–136.
- , S. Sandven, Å. Drotning, K. Kloster, T. Hamre, and M. Miles, 1997a: ERS-1 SAR sea ice catalogue. ESA SP1193, 89 pp.
- , and Coauthors, 1997b: ICEWATCH—Ice SAR monitoring of the Northern Sea route. *Operational Oceanography: The Challenge for European Co-operation*, H. W. A. Behrens et al., Eds., Elsevier Oceanography Series, No. 62, 224–233.
- Liu, A. K., B. Holt, and P. W. Paris, 1991a: Wave propagation in the marginal ice zone: Model predictions and comparisons with buoy and synthetic aperture radar data. *J. Geophys. Res.*, **96** (C3), 4605–4621.
- Liu, A. K., B. Holt, P. W. Paris and C. Y. Peng, 1991b: Observations of wave refraction at an ice edge by synthetic aperture radar. *J. Geophys. Res.*, **96** (C3), 4803–4808.
- Lyzenga, D. R., R. A. Shuchman, J. D. Lyden and C. L. Rufenach, 1985: SAR imaging of waves in water and ice: Evidence for velocity bunching. *J. Geophys. Res.*, **90** (C1), 1031–1036.
- Moore, B., and B. Bolin, 1987: The oceans, carbon dioxide and global climate change. *Oceanus*, **29**, 9–15.
- Muench, R. D., S. Martin, and J. Overland, Eds, 1987: Preface: Second marginal ice zone research collection. *J. Geophys. Res.*, **92**, 6715.
- Petterrsson, L. H., S. Sandven, Ø. Dalen, V. V. Melentyev, and N. I. Babich, 1999: Satellite radar ice monitoring for ice navigation of the ARCDEV tanker convoy in the Kara Sea. *Proc. of 15th Int. Symp. on Port and Ocean Engineering under Arctic Conditions*, Helsinki, Finland, 141–153.
- Sandven, S., O. M. Johannessen, and J. A. Johannessen, 1991: Mesoscale eddies and chimneys in the marginal ice zone. *J. Mar. Syst.*, **2**, 195–208.
- , Ø. Dalen, M. Lundhaug, K. Kloster, V. Y. Alexandrov, and L. V. Zaitsev, 2001: Sea ice investigations in the Laptev Sea area in late summer using SAR data. *Can. J. Remote Sens.*, **27**, 502–516.

Processes at the Ice Edge – The Arctic

- Shuchman, R. A., 1990: The use of synthetic aperture radar to map the Polar Oceans. *Proc. Oceans '90 Symp.*, Washington, DC, ERIM, 402–409.
- , and Coauthors, 1987: Remote sensing of the Fram Strait marginal ice zone. *Science*, **236**, 429–431.
- , C. Rufenach, and O. M. Johannessen, 1994: Extraction of marginal ice zone thickness using gravity wave imagery. *J. Geophys. Res.*, **99** (C1), 901–918.
- , and Coauthors, 1996: The Greenland Sea odden: Intra- and inter-annual variability. *Proc. SPIE*, **2959**, 242–252.
- Stouffer, R., S. Manabe, and K. Bryan, 1989: Interhemispheric asymmetry in climate response to a gradual increase of atmospheric CO₂. *Nature*, **342**, 660–682.
- Wadhams, P., 1986: The seasonal ice zone, *The Geophysics of Sea Ice*, N. Untersteiner Editor., Plenum, New York pp. 824-991
- Wadhams, P., and B. Holt, 1991: Waves in frazil and pancake ice and their detection in Seasat synthetic aperture radar imagery. *J. Geophys. Res.*, **93** (C5), 8835–8852
- WMO, 1970: *WMO Sea-Ice Nomenclature*. WMO 259, TP 145, Secretariat of the World Meteorological Organization, Geneva, Switzerland, 147 pp.